Characterization of Translocation of Silver Nanoparticles and Effects on Whole-Genome Gene Expression Using an *In Vitro* Intestinal Epithelium Coculture Model

Hans Bouwmeester,* Jenneke Poortman, Ruud J. Peters, Elly Wijma, Evelien Kramer, Sunday Makama, Kinarsashanti Puspitaninganindita, Hans J. P. Marvin, Ad A. C. M. Peijnenburg, and Peter J. M. Hendriksen

RIKILT, Institute of Food Safety, Wageningen University and Research Center, Akkermaalsbos 2, P.O. Box 230, 6700 AE Wageningen, The Netherlands

ABSTRACT Applications of nanoparticles in the food sector are eminent. Silver nanoparticles are among the most frequently used, making consumer exposure to silver nanoparticles inevitable. Information about uptake through the intestines and possible toxic effects of silver nanoparticles is therefore very important but still lacking. In the present study, we used an *in vitro* model for the human intestinal epithelium consisting of Caco-2 and M-cells to study the passage of silver nanoparticles and their ionic equivalents and to assess their effects on whole-genome mRNA expression. This *in vitro* intestine model was exposed to four sizes of silver nanoparticles for 4 h. Exposure to silver ions was included as a control since 6−17% of the silver nanoparticles were found to be dissociated into silver ions. The amount of silver ions that passed the Caco-2 cell barrier was equal for the silver ion and nanoparticle exposures. The nanoparticles induced clear changes in gene expression in a range of stress responses including oxidative stress, endoplasmatic stress response, and apoptosis. The gene expression response to silver nanoparticles, however, was very similar to that of $AgNO_3$. Therefore, the observed effects of the silver nanoparticles are likely exerted by the silver ions that are released from the nanoparticles.

KEYWORDS: silver nanoparticles · *in vitro* · oral · translocation · Caco-2 · microarray

The use of nano-based consumer products is growing rapidly, and many of such products are available in the market. To date, more than 600 consumer products that are self-identified by the manufacturers as containing nanotechnology are included in a public database.[1] Applications in the food sector are eminent, widely discussed, and cover many aspects such as improving food packaging materials, efficient nutrient delivery, formulations with improved bioavailability, and new tools for molecular and cellular detection of contaminants.[2−5]

Nanoparticles, as a consequence of their small size, exhibit different physicochemical properties and biological effects compared to their respective bulk materials, even at the same mass dose.[6] A nanoparticle is generally defined as a discrete entity that has three dimensions on the order of 100 nm or less.[7] Various types of nanoparticles are used in the food sector. With respect to inorganic nanoparticles, various metal oxides like magnesium oxide, titanium dioxide, silicon dioxide, and silver are used in, for example, coatings of food packaging materials. Notably, the conventional forms of magnesium oxide, titanium dioxide, silicon dioxide, and silver are permitted food additives (*e.g.*, E530, E171, E551, E174),[2] but without a definition of the sizes of the materials. For example, recently, we showed that silicon dioxide (E551) as used in food products contains particle sizes in the nanorange.[8] Silver (E174) is only limitedly used as food additive (as colorant). If total use, including in food packaging materials, is considered, silver nanoparticles are among the most frequently used nanoparticles, mainly because of its antimicrobial action.[9,10] In conclusion, consumer exposure to nanoparticles is inevitable, and it is therefore necessary to assess the health impact of human exposure to nanoparticles.[4,11]

Only a few oral repeated dose studies using silver nanoparticles are available (reviewed in refs 12 and 13). Kim and coworkers exposed rats orally for 28 consecutive days to high doses of silver nanoparticles (30, 300, or 1000 mg/kg/day), resulting in an increased silver content in various organs. The liver appeared to be the main accumulating organ for silver nanoparticles.[14] This was confirmed in a 90 day study from the same authors.[15] So far, these are the only oral *in vivo* studies using silver

* Address correspondence to hans.bouwmeester@wur.nl.

Received for review February 22, 2011 and accepted April 11, 2011.

Published online April 11, 2011
10.1021/nn2007145

nanoparticles. The usefulness of these studies for risk assessment is, however, rather limited since the nanoparticles as administered to the rats were not characterized (characterization in the food matrix is essential because the matrix might affect its properties: *e.g.*, agglomeration state), and a control using the conventional form of silver (Ag^+) was lacking.

The mechanism of translocation of nanoparticles over the gastrointestinal wall is poorly known. The intestinal epithelium consists of a monolayer of predominantly enterocytes, with in specific regions specialized cells for the translocation of particulate matter: epithelial M-cells.[16,17] Translocation of particles through the intestinal wall is a multistep process, involving diffusion through the mucus lining of the gut wall, contact with enterocytes and particularly the M-cells, and finally uptake *via* cellular or paracellular transport.[18] Translocation of nanoparticles through the epithelium depends on their physicochemical properties, such as size, surface charge, lipophilicity/hydrophilicity, presence/absence of a ligand, and physiology of the intestinal tract, for example, healthy *versus* diseased state.[19]

To study the mechanism of translocation, several *in vitro* models for the intestinal epithelium have been developed. Generally, models use monolayers of Caco-2 cells, but recently, more sophisticated coculture models employing M-cells are emerging. In our studies, we adopted the *in vitro* model system as developed by Des Rieux and co-workers.[20] This model is based on a coculture on inverted transwell inserts of Caco-2 cells and human Raij B lymphocytes. The setup of the system allows a close contact between the two cell types to trigger the conversion of Caco-2 cells into M-cells. The authors showed an M-cell conversion rate of 15−30% by means of scanning electron microscopy.[20] This *in vitro* coculture model has great potential for the combined detection of toxic effects and translocation properties of compounds or nanoparticles. The present study aimed to answer two questions. First, do silver nanoparticles exert nanospecific toxic effects on the cells of the *in vitro* system, and second, do these nanoparticles pass the *in vitro* intestinal barrier. In our studies, we used well-characterized silver nanoparticles of four different sizes (ranging between 20 and 110 nm) as well as $AgNO_3$ in order to compare the effects of nanoparticles with those induced by Ag^+ ions. We employed a full genome transcriptomics approach to screen for potential toxic effects.

RESULTS

Characterization of Silver Nanoparticles. Sizes of silver nanoparticles as derived from transmission electron microscopy (TEM) images were 31 ± 5, 30 ± 4, 69 ± 7, and 112 ± 9, while the sizes provided by the producer based on TEM analysis were 20 ± 2, 34 ± 3, 61 ± 5, and 113 ± 8, respectively. Throughout the paper, we will use the TEM sizes given by the producer. Representative TEM pictures are shown in Figure 1. In water at t = 0 h, the hydrodynamic sizes as determined by nanoparticle tracking analysis (NTA) of the 34, 61, and 113 nm nanoparticles were only slightly larger than that of the TEM sizes (Table 1). However, sizes determined by NTA for 20 nm TEM nanoparticles were much larger: 70.0 ± 2.0 nm. At sizes smaller than 30 nm, output of NTA might be affected by a large measurement uncertainty because the detection limit of the NTA is around 30 nm and the bias of NTA is toward larger size fractions.[21] This might partly explain the large NTA measures for the 20 nm (TEM) nanoparticles.

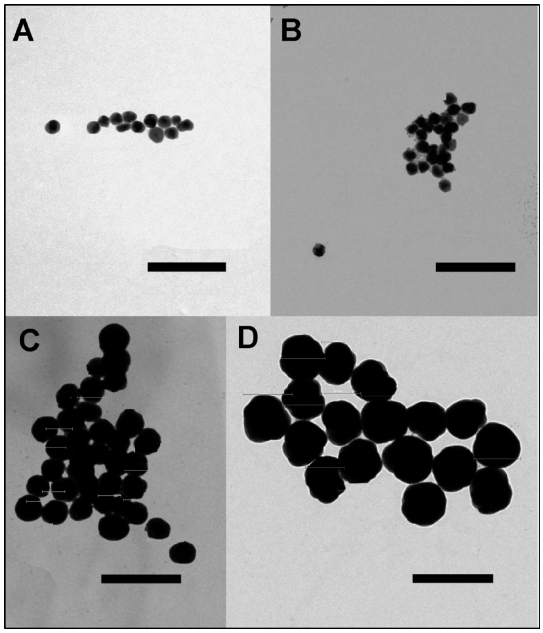

Figure 1. Transmission electron microscope (TEM) images of various silver nanoparticles in MQ water: (A) 20 nm; (B) 34 nm; (C) 61 nm; (D) 113 nm. Sizes are according to the information of the provider. Scales are 200 nm.

Compared to water, suspending the nanoparticles in cell culture medium (DMEM plus FCS) resulted in larger hydrodynamic sizes for each of the four NPs at t = 0 h already (Table 1). Compared to t = 0 h, t = 24 h of incubation resulted in larger hydrodynamic sizes, both in MQ water and even larger in cell culture medium, that is, 148.7 ± 6.8, 174.7 ± 6.8, 214.0 ± 9.2, and 232.7 ± 5.5 nm for 20, 34, 61, and 113 nm NPs, respectively. After 24 h, NTA sizes in MQ water of the 20 nm (TEM) nanoparticles were comparable to those of the 34 nm (TEM) nanoparticles. A brief sonication procedure slightly decreased the hydrodynamic sizes, but not to the original size as measured at t = 0 h (Table 1).

Chemical composition of silver suspensions (in cell culture medium) was analyzed by full spectrum ICPMS. The composition was compared with control cell culture medium. We found no impurities in the silver nanoparticle suspensions (data not shown).

TABLE 1. Sizes of Silver Nanoparticles As Determined by TEM or NTA in MQ Water and Complete Cell Culture Medium at 0 and 24 h[a]

		solvent						
		MQ water				DMEM +++		
		TEM (nm)	NTA (nm)					
compound	producer TEM (nm)	$t = 0$	$t = 0$	$t = 24$	$t = 24 + S^b$	$t = 0$	$t = 24$	$t = 24 + S^b$
	20 ± 2	31 ± 5	70 ± 2	117 ± 11	94 ± 4	93 ± 11	149 ± 6	118 ± 8
	34 ± 3	30 ± 4	47 ± 5	133 ± 12	122 ± 8	104 ± 11	175 ± 7	140 ± 12
	61 ± 5	69 ± 7	67 ± 4	182 ± 8	138 ± 10	115 ± 7	214 ± 9	148 ± 7
	113 ± 8	112 ± 9	115 ± 6	186 ± 10	177 ± 8	173 ± 8	233 ± 6	189 ± 8

[a] Note: Data are presented as mean ± SEM. [b] Time (t) = 24 h followed by a sonication procedure as described in the Materials and Methods section.

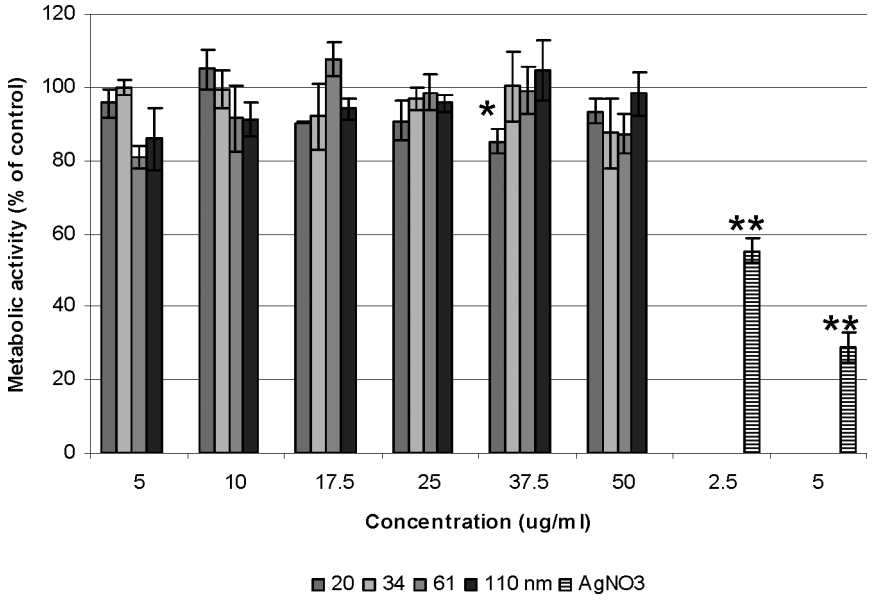

Figure 2. Viability of Caco-2 cells after exposure for 24 h to 20, 34, 61, and 113 silver nanoparticles and 2.5 and 5 μg/mL $AgNO_3$ as measured by the WST assay. Data are expressed as mean ± SEM for triplicate exposures; *$p < 0.05$; **$P < 0.001$.

Silver nanoparticles are known to release Ag^+ ions in suspensions. Therefore, the fraction of nanoparticles and Ag^+ ions was determined by ICPMS in both fresh and 24 h aged cell culture medium in which the silver nanoparticles were spinned down by double ultracentrifugation. The elementary silver present in the supernatant was most likely Ag^+, and the amount was clearly correlated to the size of the NPs. Suspensions of the smaller-sized silver nanoparticles contained relatively more ions than suspensions with larger nanoparticles: 17.4, 15.8, 5.8, and 7.6% for 20, 34, 61, and 113 nm NPs, respectively. The control supernatants provided by Nanocomposix collected immediately after production contained no or very low levels (<LOD) of elementary silver.

Viability of Caco-2 Cells Following Exposure to Silver Nanoparticles. No statistical significant treatment effects were observed, with the exception of the 20 nm silver nanoparticles at 37.5 μg/mL ($p = 0.004$). None of the nanoparticle treatments induced a reduction of viability above 20% as compared to the control group. In addition, impairment of viability was not correlated to the doses, suggesting the significant effect to be a minor incident. $AgNO_3$, on the other hand, both at the 2.5 and 5 μg/mL doses, significantly ($p < 0.001$) reduced the viability of the Caco-2 cells (Figure 2).

Validation and Characterization of the *In Vitro* Model for the Human Intestinal Epithelium. To test the barrier function of the monolayer of Caco-2 and M-cells (*e.g.*, tight junction integrity), the translocation of the paracellular transport markers Lucifer Yellow and 4 and 10 kDa dextrans was evaluated in HBSS in the presence or absence of EGTA, a calcium chelator that opens tight junctions.[22,23] If converted into the apparent permeability (Papps; cm/s) the Papps of 4 and 10 kDA dextrans are in the range (10^{-6} cm/s) as reported in

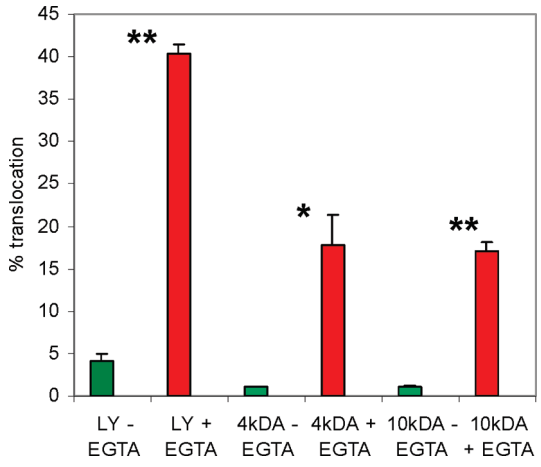

Figure 3. Monolayer integrity of the *in vitro* model. Addition of EGTA induced a significant increase in the translocation rate of Lucifer Yellow (LY), 4 kDa FTIC dextran (4 kDA), and 10 kDa FITC-dextran (10 kDa). Data are expressed as mean ± SEM; *$p < 0.005$; **$p < 0.001$.

the literature for Caco-2 cell monolayers with good tightness.[24] Addition of EGTA induced a significant increase in the translocation of Lucifer Yellow ($p < 0.001$), 4 kDa FITC-dextran ($p = 0.005$) and 10 kDa FITC-dextran ($P < 0.001$), demonstrating the functionality of the tight junctions in the monolayer (Figure 3).

The transepithelial electrical resistance was measured in all transwells. TEERs reached a plateau at the end of the culturing period (data not shown). The TEERs clearly dropped ($p \leq 0.001$) following EGTA treatment. TEER ranged between 539 and 590 $\Omega \cdot cm^2$ before EGTA treatment and decreased to 114–131 $\Omega \cdot cm^2$ after EGTA treatment. This is in agreement with the passage of Lucifer Yellow and FITC-dextran. The presence of M-cells was verified by immunohistochemistry, by using the M-cell-specific marker anti-galectin 9 (Figure 4).

Whole-Genome Gene Expression: Significantly Affected Genes. The *in vitro* model was exposed to four sizes of silver nanoparticles. In addition, cells were exposed to 1.5 μg/mL $AgNO_3$. The latter concentration was chosen because it reflects the amount of silver ions present in the silver nanoparticle suspensions used in the experiments. To obtain an impression of the number of genes affected per treatment, SAM analysis was performed using a false discovery rate of 0%. As shown in Table 2, the supernatants of the silver nanoparticles did not significantly affect any genes. The number of spots affected by the silver nanoparticles varied between the treatments from 2 and 80. No genes were detected that were significantly down-regulated during the exposure period of 4 h. In total, 128 spots (97 genes) were significantly affected by at least one treatment, and a hierarchical cluster picture for these spots is shown in Figure 5. This cluster picture shows that, although many genes did not reach significance according to SAM analysis, most of them are at least to some extent up-regulated by all NP treatments as well as by ionic silver ($AgNO_3$). The lack of significance in a part of the treatments is likely due to variation within the triplicates. A proportion of the significant genes is a little up-regulated by the supernatants of the NPs, although mostly with a lower induction factor. The lack of difference between silver ions and silver NPs implies that no genes were specifically affected by a "nanoparticle effect".

Whole-Genome Gene Expression: Biological Interpretation. Two approaches were used to acquire insight into the biological effects of the silver nanoparticles and ions. First, Metacore was used to obtain functional information about the SAM significant genes. The processes for which the SAM significant genes were highly over-represented ($P < 0.0001$) included AP1 activation, glutathione biosynthesis, "endoplasmatic reticulum (ER) and unfolded protein response", mitochondrial apoptosis, mitosis, and response to chemical stimulus. We extended this analysis by acquiring functional information for each of the SAM significant genes using Metacore, Source, and, if necessary, literature study. Functional information could be attained for 79 genes, and this is summarized in Table 3. The genes have been described as being involved in processes such as proliferation (23), response to oxidative stress (20), metal ion binding (19), unfolded protein response or ER stress (9), apoptosis (9), cell structure and migration (8), other stress responses (6), and other functions (5). Part of the genes play a role in two processes.

The induction of 19 genes involved in metal binding suggests that at least part of the significant genes specifically responds to the metal exposure. To investigate this, we assessed the expression of the 97 genes that previously were found to be significantly differentially expressed upon exposure of Caco-2 cells to the marine toxins azaspiracid-1 (AZA1), okadeic acid (OA), and dinophysistoxin-1 (DTX1). These latter data were obtained using the same microarray platform as described in the present study (Hendriksen *et al.*, personal communication). These experiments with marine toxins were done on 2–3 days cultured Caco-2 cells and differ therefore from the Caco-2 cells used for the nanoparticle study which were cultured for 21 days in the presence of Raji cells. The majority of the genes (82 of 97) up-regulated in the present study were also up-regulated in the exposure experiments with OA, DTX1, and/or AZA1.

Silver Translocation. We assessed the translocation of a selection of the silver nanoparticles following 4 h of exposure. For this, we focused on the two smallest-sized silver nanoparticles (20 and 30 nm) because we expected the smallest particles to have the highest translocation rate. $AgNO_3$ was included as a control for the ionic form of silver. Silver was measured as elementary silver by ICPMS. Translocation rates were not statistically different for the silver nanoparticles or ionic silver (Figure 6). In addition, the integrity of the monolayer of cells was

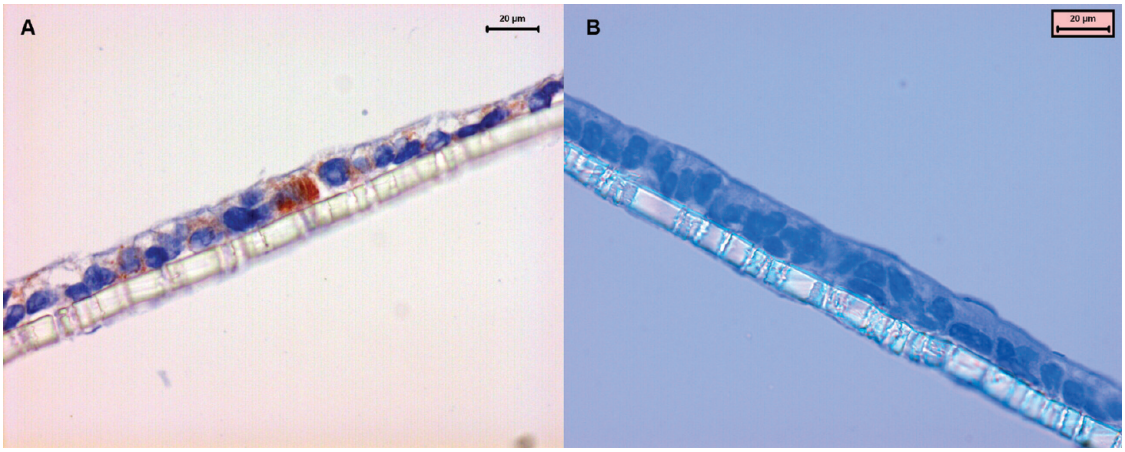

Figure 4. Immunohistochemical picture indicating the presence of M-cells in the coculture of Caco-2 and Raij-B cells on a transwell membrane. M-cells are stained using the specific antibody anti-galactine-9 (brown, see white arrow). A) Coculture of Caco-2 and Raij-B cells, B) monoculture of Caco-2 cells.

TABLE 2. Significant Genes Affected Per Treatment[a]

treatment (μg/mL)	20 nm	34 nm	61 nm	113 nm	$AgNO_3$
supernatant control[b]	0	0	0	0	
1.5					19
5	80	28	20	2	
25	14	14	37	58	

[a] Significance was assessed by SAM analysis (Tusher *et al.*, 2001); all significant genes were up-regulated. Sizes of the nanoparticles are indicated. [b] Supernatant is the fluid in which the nanoparticles were provided.

not affected by any of the exposures: TEER values before and after the silver exposure were comparable (Table 4).

DISCUSSION

In this study, we report the effects of four sizes of silver nanoparticles and silver ions on whole-genome gene expression of a coculture *in vitro* model for the human intestinal wall. We used silver nanoparticles because these are widely used in commercial products and readily available. Our most striking observation was the absence of nanoparticle-specific effects on gene expression, indicating no nanoparticle-related toxicity. Silver nanoparticle suspensions and $AgNO_3$ induced the same set of genes. It is important to note that 6−17% of the silver in the silver nanoparticle suspensions was in ionic form. This makes it very likely that the gene expression changes induced by silver nanoparticle suspensions are due to the silver ions, while the contribution of the nanoparticles themselves is very limited or absent. In addition, we show that the amount of silver that translocates over the *in vitro* monolayer during exposure to silver nanoparticles or silver ions is comparable. This indicates that the contribution of silver nanoparticles to the total of translocated silver is very limited.

Nanotoxicological data are of value for risk assessment only if the exposure is well-characterized, standardized, and clearly described dispersion protocols are used.[25−27] Also, the inclusion of an ionic control group in experiments is an important prerequisite for studies on risk assessment.[12] In the design of our experiments, we took these recommendations into account. TEM analysis of the nanoparticle suspensions revealed that the sizes of the two smallest silver nanoparticles (20 and 30 nm according to producer specifications) were overlapping (*e.g.*, 31 ± 5 and 30 ± 4), while the size distributions of the 60 and 110 nm nanoparticles (*e.g.*, 69 ± 7 and 112 ± 9) were clearly separated from each other. Likely, the differences between our own observations and the manufacturer's information are due to batch-to-batch variation or changes in material properties between initial characterization and final use. TEM analysis alone cannot provide an accurate insight in the dispersion characteristics of nanoparticles in complete cell culture medium, due to the drying of the suspensions and salt precipitation for imaging under high vacuum conditions. Therefore, we utilized NTA to determine the nanoparticle size distribution in suspensions. Hydrodynamic sizes of the silver nanoparticles were larger in the cell culture medium than in MQ water, which confirms earlier observations.[27,28] Clearly, hydrodynamic sizes of the smallest particles increase more than the sizes of the larger nanoparticles. This increase is time-dependent. Hydrodynamic sizes are larger after 24 h of incubation as compared to fresh suspensions, while brief sonication results in slightly smaller sizes. The larger hydrodynamic size of silver nanoparticles in cell culture medium compared to MQ water is likely due to the formation of a biomolecular corona.[29] It is therefore important to characterize nanoparticle properties not only in water but also in complex cell culture medium.

We detected a considerable dissociation of silver ions from the silver nanoparticles, 17% from the 20 and 34 nm sized nanoparticles and 6% from the 61 and 113 nm sized nanoparticles. Dissociation of silver ions from silver nanoparticles has been reported before.[30−32]

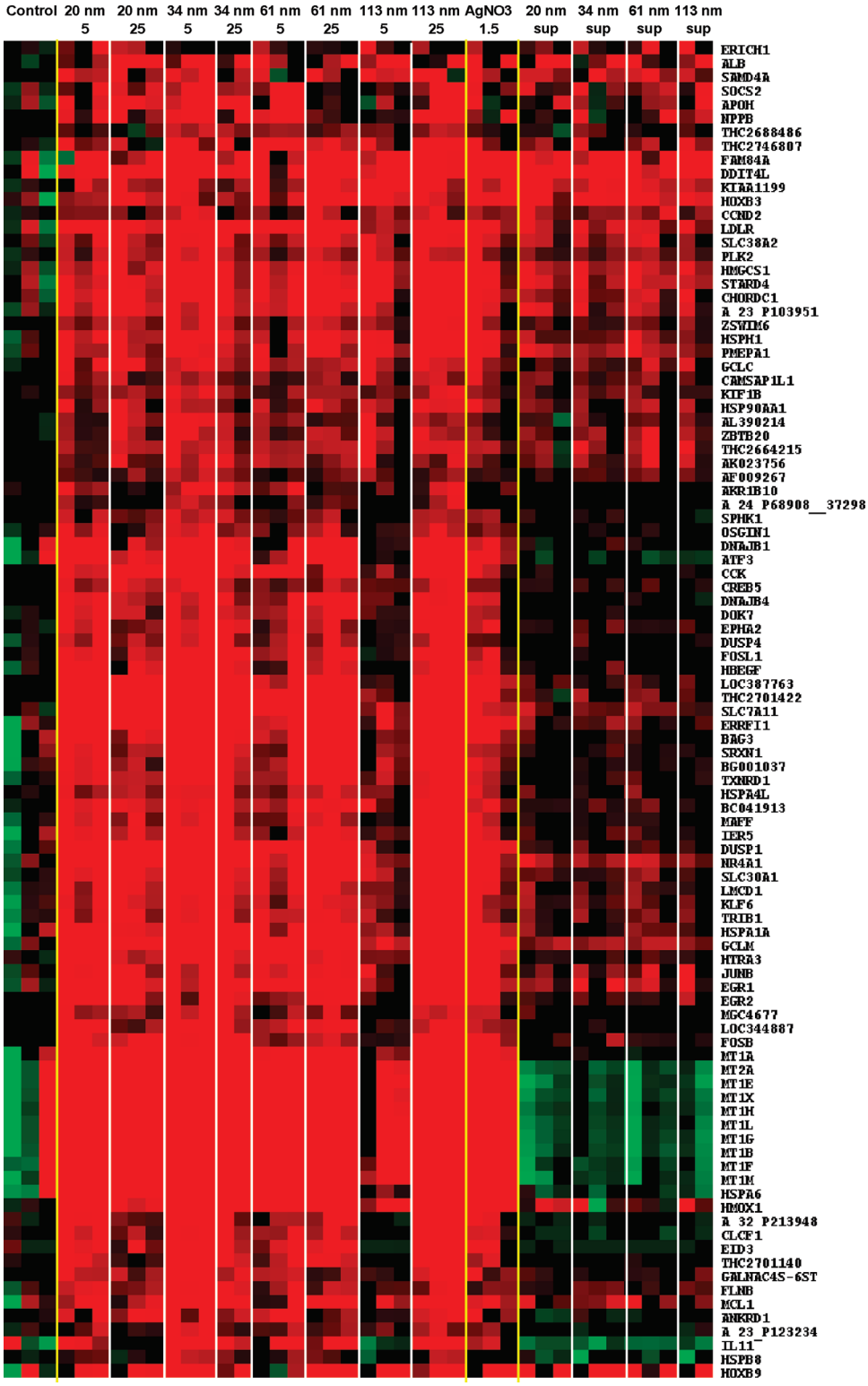

Figure 5. Hierarchical clustering of silver nanoparticles affected genes. A total of 128 spots were affected by at least one treatment. Duplicate spots for the same gene were removed. The remaining 97 genes were clustered on the differences in expression levels between treatment and the average of the control samples. Red: upregulated *vs* controls; green: downregulated *vs* controls. The sizes of the nanoparticles are indicated in nm; 1.5, 5 and 25 refer to the exposure doses in μg/mL; sup: the fluid in which the nanoparticles were provided.

As a consequence, exposure to 20 and 34 nm NPs resulted in silver ion concentrations of 0.85 and 4.25 μg/mL, while the 61 and 113 nm sized nanoparticles resulted in silver ion concentrations of 0.3 and 1.5 μg/mL for the low and high dose, respectively. These silver ion concentrations are around the

TABLE 3. Genes Significantly Affected After 4 h Exposure to Silver Nanoparticles[a]

gene symbol	highest induction value[b]	ER stress/unfolded protein response	response to oxidative stress	other stress response	apoptosis[c]	proliferation[c]	metal ion binding	cell structure and migration	other
HSPA6	17.5	+							
MT2A	10.0		+				+		
MT1G	8.8		+				+		
MT1M	8.3		+				+		
MT1L	8.2		+				+		
MT1B	8.2		+				+		
MT1E	7.9		+				+		
MT1X	7.3		+				+		
MT1H	6.8		+				+		
MT1F	6.5		+				+		
HMOX1	5.9		+						
ATF3	4.1					+			
ALB	3.9		+						
SLC7A11	3.7								amino acid and ion transport
ERRFI1	3.6					+/−			
HSPA1A	3.4	+							
BAG3	3.3				−				
DUSP1	3.3		+						
IL11	3.2					+			
NR4A1	3.2				+				
MT1A	3.1		+				+		
EGR1	3.0					+			
CCK	2.9				+				
GCLM	2.8		+						
APOH	2.8				−				
EID3	2.7								transcription inhibitor
DNAJB1	2.7	+							
LDLR	2.6								cholesterol uptake
EGR2	2.5					+			
HTRA3	2.4			+					
FOSB	2.4					+			
JUNB	2.4					+			
SLC30A1	2.4						+		
CLCF1	2.4				−				
HOXB3	2.3							+	
SOCS2	2.3					−			
HOXB9	2.3							+	
MCL1	2.3				+/−				
FAM84A	2.3							+	
HBEGF	2.3					+			
NPPB	2.3					−			
TRIB1	2.3					−			
SRXN1	2.3		+						
KIAA1199	2.2					+			
CHORDC1	2.2						+		
FOSL1	2.2					+			
IER5	2.2					−			
LMCD1	2.2						+		
DDIT4L	2.2			+					
HMGCS1	2.2								cholesterol biosynthesis
STARD4	2.2	+							
MAFF	2.2			+					
KLF6	2.1					−	+		
GALNAC4S-6ST	2.1							+	
TXNRD1	2.1		+						
PMEPA1	2.1					−			
HSPH1	2.1	+							
EPHA2	2.0				+				

TABLE 3. Continued

gene symbol	highest induction value[b]	ER stress/unfolded protein response	response to oxidative stress	other stress response	apoptosis[c]	proliferation[c]	metal ion binding	cell structure and migration	other
AKR1B10	1.9		+						
DNAJB4	1.9	+							
SLC38A2	1.9								amino acid and ion transport
DOK7	1.9							+	
DUSP4	1.9		+						
ANKRD1	1.9			+					
FLNB	1.9							+	
SAMD4A	1.9					−			
HSP90AA1	1.8	+							
HSPA4L	1.8	+							
ZSWIM6	1.8						+		
CREB5	1.8						+		
KIF1B	1.8							+	
GCLC	1.8		+						
ZBTB20	1.7						+		
PLK2	1.7					+			
OSGIN1	1.7					−			
CCND2	1.7					+			
HSPB8	1.7					−			
SPHK1	1.6					+			
CAMSAP1L1	1.6							+	

[a] Significance was determined by SAM analysis; genes without functional information are not shown. [b] The numerical ratio is given for the silver nanoparticle treatment (average of a triplicate) with the highest induction value. [c] The + and − indicate positive or negative regulation of apoptosis or proliferation.

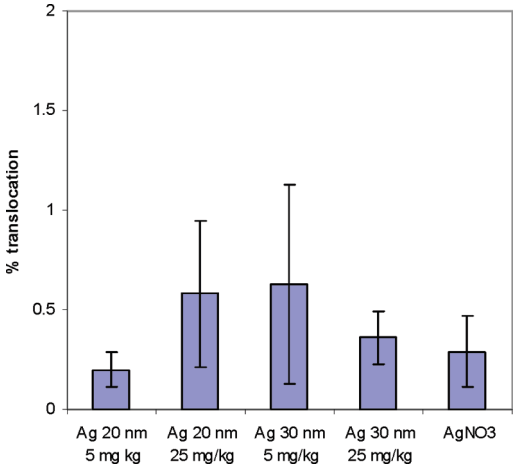

Figure 6. Translocation of silver following exposure of coculture monolayer for 4 h to silver nanoparticles or $AgNO_3$. Accompanying TEER values before and after each exposure are presented below each respective bar. Results are presented as mean ± SEM.

dose of $AgNO_3$ (1.5 μg/mL) used in our transcriptomics and translocation study.

It was important to expose the Caco-2 cells to noncytotoxic doses of nanoparticles to avoid disruption of the coculture monolayer of cells and generation of low-informative gene expression profiles related to cell death. Potential induction of cytotoxicity was therefore tested on proliferating Caco-2 cells using the WST-1 assay that gives a measure for mitochondrial activity. None of the doses tested resulted in an altered mitochondrial activity after 24 h of exposure. However,

TABLE 4. Membrane Integrity Following Exposure to Silver Nanoparticles and $AgNO_3$

	TEER[a] ($\Omega \cdot cm^2$) ± SEM				
	Ag 20	Ag 20	Ag 30	Ag 30	$AgNO_3$
dose (μg/mL)	5	25	5	25	1.5
before	440 ± 51	412 ± 55	428 ± 5	406 ± 46	464.3 ± 29
after	529 ± 51	530 ± 56	510 ± 32	577 ± 19	530 ± 89
Δ%	17 ± 6	22 ± 9	16 ± 7	30 ± 8	11 ± 13

[a] TEER before and after each exposure are presented as mean ± SEM.

$AgNO_3$ at concentrations of 2.5 and 5 μg/mL decreased cell viability. In the translocation study, none of the exposures resulted in disruption of the monolayer, as shown by unaffected TEER. The concentration of $AgNO_3$ (1.5 μg/mL) used for the translocation and gene expression study was lower than that used for the viability assay.

From the several *in vitro* models for the human gastrointestinal wall that have been developed,[36,37] we adopted the coculture model of Des Rieux.[20] The induction of differentiation of part of the Caco-2 cells into M-cells results in a more effective and more *in vivo*-like intestine translocation model. For example, the combination of Caco-2 cells and M-cells transports polystyrene nanoparticles (>200 nm) at a 50-fold higher rate than a monoculture of Caco-2 cells.[20] In our study, we confirmed the basic characteristics of the model: the presence of M-cells and integrity and functionality of the model. Initial translocation of Lucifer Yellow and dextrans

was very limited, showing the integrity of the monolayer. Opening the tight junction by EGTA resulted in increased translocation of the used paracellular markers and a clear drop of TEER levels confirming the physiological functionality of the coculture monolayer.

For our whole-genome gene expression analysis, we exposed the coculture model to $AgNO_3$ and four sizes of nanoparticles. Since we were mainly interested in the primary effects of the silver nanoparticles, a short exposure time of 4 h was selected. Using SAM analysis, 97 genes were found to be significantly up-regulated by at least one treatment. No gene was down-regulated, which is likely due to the short exposure time. It is a general observation that down-regulation, requiring active mRNA degradation, takes longer than up-regulation (see, for instance, ref 38).

An important aim of the microarray experiments was to detect possible nanoparticle-specific effects. However, genes affected by any of the nanoparticles were at least to some extent affected by $AgNO_3$, as well. As mentioned earlier, we detected a considerable dissociation of silver ions from the silver nanoparticles, to a level comparable with $AgNO_3$ exposures (*e.g.*, 1.5 μg/mL). It is therefore very likely that the gene expression changes are completely caused by the effect of silver ions. An alternative hypothesis is the intracellular ionization of silver nanoparticles, for example, *via* a Trojan-horse-type mechanism[13,41] and thus a constant release of ions. This, however, cannot explain our findings because then exposure to silver nanoparticles would result in stronger effects compared to the $AgNO_3$ exposures. Taken together, it implies that, at least in the present experimental setting, silver nanoparticles have no effect on the gene expression in Caco-2 cells. A same finding has been reported for the effects of tungsten carbide cobalt nanoparticles and free cobalt ions on human keratinocytes.[39] Most likely the contribution of ions to toxicity is a general rule for nanoparticles that readily dissociate toxic ions.

The functions of the genes affected by the silver nanoparticles and ions point to a series of toxic effects: oxidative stress, AP1 activation, proliferation, (mitochondrial) apoptosis, "unfolded protein response and ER stress", cell structure, and "response to chemical stimulus". The treatments highly up-regulated a group of nine metallotheinins, which are known to play an important role in both protection against oxidative stress and detoxification of metals.[40] The increased expression of genes coding for metallotheinins has also been observed for RAW264.7 cells exposed to silver nanoparticles of 70 nm for 24−96 h.[41] Two other up-regulated genes, GCLC and GCLM, are essential for the synthesis of glutathione that is involved in the protection against oxidative stress and metals, as well.[40] These genes were also affected in C17.2 neural stem cells exposed to supermagnetic iron oxide nanoparticles.[42] Exposure to silver ions (and ions from other metals) induce reactive oxygen species (ROS) which causes oxidative stress and a decrease of reduced glutathione.[43−45] The induction of ROS is attributed to two processes: (1) direct formation of ROS from O_2 *via* the Fenton reaction, and (2) increased production of ROS within mitochondria likely due to the reaction of silver ions with SH groups of enzymes belonging to the respiratory chain.[40,43,45,46]

Activation of AP1 is a well-known response to oxidative stress.[45] AP1 consists of a group of proteins from which FOSB, FOSL1, and JUNB were among the up-regulated genes in our experiment. Dependent on the context, AP1 can either positively of negatively affect the cell proliferation.[45,47] In addition, AP1 activation can induce the expression of apoptosis-related genes.[45,47] Silver ions also have a direct effect on mitochondria leading to cytochrome *c* release,[46] which is a second route inducing apoptosis. This is in agreement with the induction of many proliferation- and apoptosis-related genes in our experiment. In the literature, we could not find other studies reporting that silver induces ER stress. The induction of ER stress, however, has been described for other metals, including cadmium, lead, and titanium.[48−50] We made an important observation that 80% of the genes up-regulated by silver nanoparticle suspensions are also up-regulated by one or more of the nonmetal compounds AZA1, OA, or DTX1, which are marine biotoxins under investigation in our group. This demonstrates that the silver nanoparticle suspensions exert general stress responses rather than specific nanometal responses.

Toxic effects of silver nanoparticles *in vitro* have been described for cell types other than Caco-2 cells. Exposure of rat liver cells to 15 and 100 nm silver nanoparticles increased lactate dehydrogenase leakage and inhibited mitochondrial function at $\geq$5 and $\geq$10 μg/mL, respectively.[33] In mouse germline stem cells, silver nanoparticles (15 nm) at 5 and 10 μg/mL impaired cell proliferation and induced cytotoxicity, while silver carbonate at a same and higher concentration had no effect.[34] On human HepG2 cells, both 7 and 10 nm silver nanoparticles (stabilized with polyethylenimine) and Ag^+ ions (from Ag_2CO_3) induced toxic effects following 24 h exposure. Concentrations higher than 1 μg/mL resulted in cytotoxicity, while at lower levels, cell proliferation was induced. This was confirmed by microarray data, revealing significant induction of genes associated with cell cycle progression.[35] Taken together, silver nanoparticles negatively affect cell proliferation and induce cytotoxicity in different cell lines, although this may also be due to differences in the nature of the silver nanoparticles.

Our translocation experiments clearly show that silver derived from either silver nanoparticle suspensions or $AgNO_3$ can pass the coculture cell barrier. Strikingly, no significant translocation differences between nanoparticle suspension or $AgNO_3$ were found.

A prominent question is the nature of the translocated silver: as nanoparticle or in the ionic form. In our current study, silver was detected by ICPMS or AAS. In this procedure, all silver is dissociated with HNO_3 to elementary silver. We have therefore no information about the nanoform. The amount of silver that translocated through the Caco-2 cell barrier was equal for the silver ion and nanoparticle exposures. The silver ion and nanoparticle suspensions contained about the same silver ion concentration. When next to silver ions also silver nanoparticles would have translocated, more translocated silver would be expected for the nanoparticle suspensions than for the ions. This was, however, not the case. Therefore, the translocation of silver is likely to be in the ionic and not in the particulate form.

The present study was the first in which translocation of silver nanoparticles was studied using an *in vitro* model of the gastrointestinal wall. This *in vitro* culture system as model for the human intestinal epithelium proves to be an elegant system to be used in a tiered-risk assessment approach. In this study, silver nanoparticles and its ionic equivalent were used as model compounds. Characterization of the nanoparticle suspensions revealed the presence of free silver in the nanoparticle suspensions. It is likely that both the gene expression changes and the translocation of silver over the *in vitro* intestine model can be solely explained by the presence of free silver, without any additional effect of the nanoparticles. This indicates that the presence of silver ions in silver nanoparticle suspension is of more toxicological concern than the silver nanoparticles themselves.

MATERIALS AND METHODS

Cell Lines and Culture Media. Human colon (colorectal adenocarcinoma) Caco-2 cell line (HTB-37TM) and human Burkitt's (lymphoma cells) Raji B line (CCL-86TM) were obtained from American Type Culture Collection, Manassas, VA (ATCC), and used at passages 25−35 and 8−29, respectively, at a seeding density of 60 000 cells/cm^2.

Caco-2 cells were cultured in BioWhittaker's Dulbecco modified Eagle's minimal essential medium (DMEM, 4.5 g/L glucose) supplemented with L-glutamine from Lonza (Verviers, BE). Raij B cells were grown in RPMI 1640 medium (Gibco). To both media we added non-essential amino acids (NEAA) from MP Biomedicals (Illkirch, France), penicillin-streptomycin (PEST; Sigma, St. Louis, MO), and heat-inactivated fetal bovine serum (FBS; 10% v/v) from Gibco. Hank's balanced salt solution (HBSS) was made by mixing Hank's balanced salt containing calcium and magnesium (Sigma-Aldrich), sodium carbonate (Merck), and Milli-Q water.

Nanoparticle Suspensions. Four sizes of silver nanoparticles (*e.g.*, 20.3 ± 1.9, 34.4 ± 3.4, 61.2 ± 5.3, and 112.6 ± 7.8 nm; TEM diameter as provided by manufacturer) were obtained from Nanocomposix (San Diego, CA) as suspensions at a concentration of 1 mg/mL in 2 mM phosphate buffer. Stock suspensions were made in complete cell culture medium. To aid dispersion, stocks were sonicated for 10 min at 20 °C using a Branson 5510 ultrasonic machine (4 W specific ultrasound energy (240 J/m^3)) and afterward diluted in DMEM, supplemented with 10% FCS, to the final exposure concentrations.

Nanoparticle Characterization. Nanoparticle tracking analysis (NTA), transmission electron microscopy (TEM), and inductively coupled plasma mass spectrophotometry (ICP-MS) techniques were used to characterize the nanoparticle suspensions. Hydrodynamic diameters were obtained following NTA (NanoSight, NanoSight Limited, Wiltshire, UK) in MQ water (pH 5.5) and DMEM containing 10% FCS. Measurements were performed at t = 0, 24, and 24 h, all at 37 °C followed by a brief sonication procedure. Each measurement was perfomed in triplicate, and hydrodynamic diameters were obtained using Nano Track Analysis software (NTA 1.5).

To determine the morphological characteristics of the nanoparticles, TEM pictures were made using a JEOL JEM 1011 microscope, delivering beam current at 045 A and fitted with a Keenview 1k × 1k camera. Grids were prepared on Cu mesh 400 holey carbon film. Nanoparticles were viewed at a concentration of 10 μg/mL to achieve optimal surface coverage. About 5 μL was dropped on and left to dry completely. The mean ± SEM of 10 particles is reported.

Elemental analysis to determine the purity of the nanomaterial stock suspensions was performed using inductively coupled plasma mass spectrometry (ICP-MS). In addition, the ratio of Ag nanoparticles *versus* Ag^+ in the cell culture medium was determined by means of ICP-MS analysis of the supernatant after double ultracentrifugation (35 000 rpm) of the suspensions for 10 min. The ICP-MS was a Thermo Scientific Xseries 2 equipped with a Babington nebulizer and autosampler. For the determination of the purity, the ICP-MS was run in the multi-element screening mode with a mass range of m/z 7 to 250. For the determination of the Ag nanopaticles *versus* Ag^+ ratio, the ICP-MS was run in the selected element monitoring mode with m/z values of 107 and 109 for silver.

***In Vitro* Model for the Human Intestinal Epithelium.** Caco-2 cells were grown in 75 cm^2 flasks (Corning NY) in 10 mL of DMEM supplemented with 10% (v/v) fetal bovine serum (FCS) and 1% (v/v) each of NEAA and PEST. Cells were incubated at 37 °C in humidified air (95% RH) and 5% carbon dioxide (Thermo Scientific HERAcell 240). Culture medium was refreshed every other day, and at 80% confluency, the adherent cells were passed by subcultivation at ratio 1:3 or 1:4.

The inverted coculture model used was adapted from Des Rieux and co-workers.[20] Briefly, Caco-2 cells were seeded in 12-well transwell plates (Corning, NY) at a density of 80 000 cells/cm^2 (*i.e.*, 67 200 cells/insert; 1.12 cm^2 effective membrane growth area) and allowed to attach and grow for 5 days with culture media being refreshed every other day. Sterilized silicon tubes (internal diameter, 14 mm; height, 20 mm) were fixed to the basolateral part and the inserts inverted in a sterile glass cell culture dish (diameter, 245 mm; height, 20 mm). The Caco-2 cell monoculture was maintained in this inversed orientation and submerged in culture medium until day 21. The silicon (basolateral) chamber was refreshed with DMEM every other day until day 16. At day 16, Raji cells, cultured in suspension in 10% w/v FBS-enriched RPMI medium, were centrifuged at 1200 rpm (Heraeus Labofuge 400 R) for 10 min and resuspended in DMEM. Cells were counted and cocultured with Caco-2 cells by dispensing 500 μL resuspended Raji cells into the basolateral chamber of the insert (60 000 Raji cells/cm^2). The Caco-2/Raji coculture was maintained until day 21 when the exposure and translocation studies were conducted. Unless stated otherwise, all media and solutions were prewarmed to 37 °C before use.

Characterization of the *In Vitro* Model for the Human Intestinal Epithelium. The monolayer integrity was determined by measuring the transepithelial electric resistance (TEER) and by assessing the paracellular permeability of the monolayer to Lucifer Yellow (LY; mw 450) and fluorescein isothiocyantedextran

(FITC)-dextran (4 and 10 kDa). In addition, the presence of M-cells was determined immunohistochemically.

TEER measurement of cell monolayer was conducted in freshly added DMEM using Millipore Millicell-ERS for cells grown in inserts. The increase in TEER across cell monolayer was monitored every time culture medium was refreshed, until inserts were inverted and it was no longer practicable. Measurements were also taken pre- and postexposure to compounds to compare effect on tight junction. Percentage change in TEER was calculated using (Teeri − Teerp)/Teeri) × 100, where Teeri and Teerp represent the pre-exposure and postexposure TEER, respectively.

The paracellular permeability of cell monolayer was evaluated using Lucifer Yellow (low molecular weight) and FITC-dextran 4 and 10 kDa (Sigma, Steinheim, Germany) with and without treatment with 2.5 mM ethylene glycolbis(β-aminoethyl ether)-*N*,*N*,*N*′,*N*′-tetraacetic acid (EGTA; Sigma, Steinheim, Germany). EGTA was employed as a tight junction and adherens junction disruptor *via* its activation of protein kinase C and Ca^{2+} chelating effect and as such capable of increasing paracellular permeability.[51,52] EGTA solutions were prepared in HBSS for the EGTA positive groups; EFTA was added apically and basolaterally to a final concentration of 2.5 mM and incubated for 60 min. Inserts were washed with HBSS following this treatment and exposed to test compounds apically, then incubated for 90 min. Samples from both chambers in both groups were collected, and the amount Lucifer Yellow and FITC-dextran was measured by fluorimetry (BioTek synergy HT) at excitation/emission wavelength of 485/530 nm.

The results are reported as percentage of compound in the basolateral chamber from the total added compound. In addition the apparent permeabilities (Papp, cm s^{-1}) were calculated and expressed as mean SEM.

$$\text{Papp} = (\Delta Q/\Delta t) \times (A \times C_0)^{-1}$$

where $\Delta Q/\Delta t$ is the amount of silver transported to the basolateral compartment in unit of time, t (s). A is the membrane area (1.12 cm^2), while C_0 is the initial concentration in the apical compartment (1 mg/mL).

A routine primary antibody immunohistochemical staining technique was used for the identification of M-cells by using anti-galectin 954. Briefly, inserts of Caco-2/Raji cell coculture were washed with HBSS and fixed in 4% formaldehyde for 48 h before transferring to PBS and kept at 4 °C. The insert membranes bearing the cell monolayers were removed from the inserts by careful excision and placed in a fixation case to be fixed, dehydrated/rehydrated, and embedded in paraffin automatically using Tissue-Tek VIP. The staining is done automatically with BenchMark (Ventana), and it involves deparaffination and I-VIEW inhibitor steps interspaced by a mild (30 min) microwave step. The antibody directed against galectin 9[53] (R&D systems, Mineapolis, MN; 1:10 dilution) is then applied (100 μL) on slides and incubated at 37 °C for 2 h. Incubation was continued using HRP conjugated secondary antibody (igG; Vector Laboratories), and the immune reaction was visualized by incubation in 0.05% 3,3-diaminobenzidine (DAB; Sigma) dissolved in Tris-HCl (pH 7.4) containing 0.03% H_2O_2 for 8 min. Hematoxylin is used for counterstaining, giving the enterocytes a bluish background stain. Immunohistochemical staining was examined under a Zeiss Light microscope, and pictures were captured by a Leica DC 500 camera fitted to the microscope.

Viability and Toxicity Assays. To select noncytotoxic concentration range of silver nanoparticles to be used for transcriptomics and translocation studies, a WST-1 viability assay was carried out on Caco-2 cells.

Caco-2 cells were seeded in 96-well plate at a concentration of 40 000 cells/mL, 48 h before exposure. The assay used to determine cell viability was the tetrazolium salt 2-(4-iodophenyl)-3-(4-nitrophenyl)-5-(2,4-disulfophenyl)-2*H*-tetrazolium (ROCHE, Mannheim, Germany), better known as WST-1 assay. Briefly, 50 μL of the culture media was removed and replaced by 50 μL of the different concentrations of nanoparticles in a way that the final exposure media had a concentration of 5, 10, 17.5, 25, 37.5, and 50 μg/mL. In addition, $AgNO_3$ was applied to a final concentration of 2.5 and 5 μg/mL. After incubation for 24 h, the optical density (OD) was measured at 450 nm in a BioTek Synergy HT Multi-Mode microplate reader.

The percentage cell viability was calculated using the following equation:

$$\frac{\text{OD}_{\text{treated}}}{\text{OD}_{\text{solvent control}}} \times 100$$

A possible interaction in the read-out system between the silver nanoparticle suspension and formazan (reaction product in the WST-1 assay) was tested. Experiments were conducted in quadruplets (n = 4) unless stated otherwise, and results are expressed as mean ± standard error of mean (SEM).

Establishing Nanoparticle Translocation. The translocation of the four types of silver nanoparticles at concentrations of 5 and 25 μg/mL was tested during a 4 h exposure period. In addition, in separate transwells, monolayers were exposed to 1.5 μg/mL $AgNO_3$; 500 μL of each concentration was added to the apical chamber of 21 day old Caco-2/Raji cell coculture monolayer in 12-well transwell plates. Cells were incubated for 4 h. DMEM without phenol red was used as culture medium in the translocation experiments, and samples were collected from both apical and basolateral compartments of the transwell plates.

The total silver transported and contained in the cells, as well as the final silver concentration in the apical compartment, was measured using graphite furnace atomic absorption spectrometry. Samples were digested in a CEM Mars microwave digestion system and analyzed using a Perkin-Elmer AAnalyst 800 AAS. The results are reported as percentage of compound in the basolateral chamber from the total added compound. In addition, the results are reported as apparent permeabilities (Papp, cm s^{-1}).

Transcriptomic Analysis. To study the effects on the transcriptome of the cells in the monolayer, the conditions of the translocation experiments were used. Briefly, the monolayer of cells was exposed to four types of silver nanoparticles at concentrations of 5 and 25 μg/mL for 4 h. Subsequently, cells were washed to remove remaining nanoparticles, solubilized in 500 μL of TRIZOL (Invitrogen, Breda, The Netherlands), and stored at −80 °C until further use. The lysate was mixed with chloroform, centrifuged at 12 000*g* for 20 min at 4 °C, and the aqueous phase was transferred to be mixed with isopropyl alcohol, which precipitates total RNA. After centrifuging (20 min, 12 000*g* at 4 °C), the pellet was washed with 75% ethanol centrifuged at 12 000*g* for 15 min at 4 °C and resuspended in RNase-free water. Subsequently, RNA was further purified using the RNeasy Mini Kit (Qiagen, Venlo, The Netherlands). Integrity, purity, and concentration of the RNA were assessed by gel electrophoresis and spectrophotometrically at wavelengths of 230, 260, and 280 nm.

One microgram of each individual RNA sample was amplified using a low RNA input fluorescent linear amplification kit (Agilent Technologies, Amstelveen, The Netherlands). Label efficiency and yield were determined using a Nanodrop spectrophotometer (Nanodrop Technologies).

Subsequently, the common reference sample, that is, a pool of all RNAs, was labeled with Cy3, and the individual RNAs of each of the treated and control samples were labeled individually with Cy5. The labeled cRNA was purified (QIAquick spin columns, QIAGEN, Venlo, The Netherlands). Equal amounts (500 ng of each sample) of Cy5-labeled cRNA and Cy3-labeled reference cRNA were mixed. Hybridizations were carried out on the 4 × 44 K human whole-genome Agilent microarray platform following the Agilent two-color microarray-based gene expression analysis protocol. Microarray slides were incubated for 16−17 h at 37 °C in a microarray incubation chamber (Agilent) with continuous rotation. After hybridization, slides were washed using various dilutions of SSPE (sodium chloride, sodium phosphate, EDTA) buffer and dried according to the protocol provided by Agilent. Arrays were scanned using an Agilent microarray scanner (G2565B).

Feature extraction 9.1 software (Agilent Technologies) was used for quantification of spot intensities. GeneMaths XT (Applied Maths, Sint-Martens-Latem, Belgium) was used for background correction and normalization.[54] Spot intensities were floored to 120, which was followed by 2 log mean-

centering and calculation of 2 log ratios of treatments *versus* the average of the control samples.

The significant analysis of microarrays method (SAM; version 3.05[55]) was used to detect significantly differentially expressed spots between treatment groups *versus* the control group. Significant genes were selected using a false discovery rate of 0%.

Hierarchical clustering was done using the programs Cluster (uncentered correlation; average linkage clustering) and Treeview.[56]

Functional information about the significant genes was obtained through Metacore (GeneGo, St. Joseph, MI)[57] (http://source.stanford.edu) and literature study.

Statistical Analysis. All results are presented as the mean ± standard error of the mean (SEM). Statistical significance was determined *via* a parametric one-way analyis of variance (ANOVA), and post hoc Bonferroni correction was performed for multiple comparisons (SPSS). The results were considered significant if $p \leq 0.05$.

Acknowledgment. This study was supported by funding from the Dutch department of Economy, Agriculture and Innovation. The authors thank A. van Polanen, S. Oostrom, and R. Bakker.

REFERENCES AND NOTES

1. PEN Consumer Products. An Inventory of Nanotechnologybased Consumer Products Currently on the Market. Available online at http://www.nanotechproject.org, 2009.
2. Chaudhry, Q.; Scotter, M.; Blackburn, J.; Ross, B.; Boxall, A.; Castle, L.; Aitken, R.; Watkins, R. Applications and Implications of Nanotechnologies for the Food Sector. *Food Addit. Contam.* **2008,** *25*, 241–58.
3. Chen, H. D.; Weiss, J. C.; Shahidi, F. Nanotechnology in Nutraceuticals and Functional Foods. *Food Technol.* **2006,** *60*, 30–32.
4. Das, M.; Saxena, N.; Dwivedi, P. D. Emerging Trends of Nanoparticles Application in Food Technology: Safety Paradigms. *Nanotoxicology* **2009,** *3*, 10–18.
5. Weiss, J.; Takhistov, P.; McClements, J. Functional Materials in Food Nanotechnology. *J. Food Sci.* **2006,** *71*, R107–R116.
6. Oberdorster, G.; Maynard, A.; Donaldson, K.; Castranova, V.; Fitzpatrick, J.; Ausman, K.; Carter, J.; Karn, B.; Kreyling, W.; Lai, D.; *et al.* Principles for Characterizing the Potential Human Health Effects from Exposure to Nanomaterials: Elements of a Screening Strategy. *Part. Fibre Toxicol.* **2005,** *2*, 8.
7. SCENIHR Scientific Committee on Emerging and Newly Identified Health Risk SCENIHR.Opinion on: The Scientific Aspects of the Existing and Proposed Definitions Relating to Products of Nanoscience and Nanotechnologies European Commision Health & Consumer Protection Directorate-General. Directorate C - Public Health and Risk Assesment C7- Risk Assessment , 2007.
8. Dekkers, S.; Krystek, P.; Peters, R. J.; Lankveld, D. X.; Bokkers, B. G.; van Hoeven-Arentzen, P. H.; Bouwmeester, H.; Oomen, A. G. Presence and Risks of Nanosilica in Food Products. *Nanotoxicology* 2010, DOI: 10.3109/17435390.2010.519836.
9. Chen, X.; Schluesener, H. J. Nanosilver: A Nanoproduct in Medical Application. *Toxicol. Lett.* **2008,** *176*, 1–12.
10. PEN, Silver Nanotechnologies and the Environment: Old Problems or New Challenges? Available online at: http://www.nanotechproject.org/process/assets/files/7036/nano_pen_15_final.pdf, 2008.
11. Bouwmeester, H.; Dekkers, S.; Noordam, M. Y.; Hagens, W. I.; Bulder, A. S.; de Heer, C.; ten Voorde, S. E. C. G.; Wijnhoven, S. W. P.; Marvin, H. J. P.; Sips, A. J. A. M. Review of Health Safety Aspects of Nanotechnologies in Food Production. *Regul. Toxicol. Pharmacol.* **2009,** *53*, 52–62.
12. Christensen, F. M.; Johnston, H. J.; Stone, V.; Aitken, R. J.; Hankin, S.; Peters, S.; Aschberger, K. Nano-Silver Feasibility and Challenges for Human Health Risk Assessment Based on Open Literature. *Nanotoxicology* **2010,** *4*, 284–295.
13. Johnston, H. J.; Hutchison, G.; Christensen, F. M.; Peters, S.; Hankin, S.; Stone, V. A Review of the *In Vivo* and *In Vitro* Toxicity of Silver and Gold Particulates: Particle Attributes and Biological Mechanisms Responsible for the Observed Toxicity. *Crit. Rev. Toxicol.* **2010,** *40*, 328–346.
14. Kim, Y. S.; Kim, J. S.; Cho, H. S.; Rha, D. S.; Kim, J. M.; Park, J. D.; Choi, B. S.; Lim, R.; Chang, H. K.; Chung, Y. H.; *et al.* Twenty-Eight-Day Oral Toxicity, Genotoxicity, and Gender-Related Tissue Distribution of Silver Nanoparticles in Sprague-Dawley Rats. *Inhal. Toxicol.* **2008,** *20*, 575–583.
15. Kim, W.-Y.; Kim, J.; Park, J. D.; Ryu, H. Y.; Yu, I. J. Histological Study of Gender Differences in Accumulation of Silver Nanoparticles in Kidneys of Fischer 344 Rats. *J. Toxicol. Envrion. Health, Part A* **2009,** *72*, 1279–1284.
16. Gebert, A.; Bartels, H. Ultrastructure and Protein Transport of M Cells in the Rabbit Cecal Patch. *Anat. Rec.* **1995,** *241*, 487–495.
17. Gebert, A. The Role of M Cells in the Protection of Mucosal Mmembranes. *Histochem. Cell Biol.* **1997,** *108*, 455–470.
18. Hoet, P.; Bruske-Hohlfeld, I.; Salata, O. Nanoparticles—Known and Unknown Health Risks. *J. Nanobiotechnol.* **2004,** *2*, 12.
19. des Rieux, A.; Fievez, V.; Garinot, M.; Schneider, Y. J.; Preat, V. Nanoparticles as Potential Oral Delivery Systems of Proteins and Vaccines: A Mechanistic Approach. *J. Controlled Release* **2006,** *116*, 1–27.
20. des Rieux, A.; Fievez, V.; Théate, I.; Mast, J.; Préat, V.; Schneider, Y.-J. An Improved *In Vitro* Model of Human Intestinal Follicle-Associated Epithelium To Study Nanoparticle Transport by M Cells. *Eur. J. Pharm. Sci.* **2007,** *30*, 380–391.
21. Diegoli, S.; Manciulea, A. L.; Begum, S.; Jones, I. P.; Lead, J. R.; Preece, J. A. Interaction between Manufactured Gold Nanoparticles and Naturally Occurring Organic Macromolecules. *Sci. Total Environ.* **2008,** *402*, 51–61.
22. Sergent, T.; Parys, M.; Garsou, S.; Pussemier, L.; Schneider, Y. J.; Larondelle, Y. Deoxynivalenol Transport Across Human Intestinal Caco-2 Cells and Its Effects on Cellular Metabolism at Realistic Intestinal Concentrations. *Toxicol. Lett.* **2006,** *164*, 167–176.
23. Mounier, J.; Vasselon, T.; Hellio, R.; Lesourd, M.; Sansonetti, P. J. *Shigella flexneri* Enters Human Colonic Caco-2 Epithelial Cells through the Basolateral Pole. *Infect. Immun.* **1992,** *60*, 237–248.
24. Artursson, P.; Lindmark, T.; Davis, S. S.; Illum, L. Effect of Chitosan on the Permeability of Monolayers of Intestinal Epithelial Cells (Caco-2). *Pharm. Res.* **1994,** *11*, 1358–1361.
25. Bihari, P.; Vippola, M.; Schultes, S.; Praetner, M.; Khandoga, A.; Reichel, C.; Coester, C.; Tuomi, T.; Rehberg, M.; Krombach, F. Optimized Dispersion of Nanoparticles for Biological *In Vitro* and *In Vivo* Studies. *Part. Fibre Toxicol.* **2008,** *5*, 14.
26. Bouwmeester, H.; Lynch, I.; Marvin, H.; Dawson, K.; Berges, M.; Braguer, D.; Byrne, H.; Casey, A.; Chambers, G.; Clift, M.; *et al.* Minimal Analytical Characterisation of Engineered Nanomaterials Needed for Hazard Assessment in Biological Matrices. *Nanotoxicology*, **2010**, DOI: 10.3109/17435391003775266.
27. Murdock, R. C.; Braydich-Stolle, L.; Schrand, A. M.; Schlager, J. J.; Hussain, S. M. Characterization of Nanomaterial Dispersion in Solution Prior to *In Vitro* Exposure Using Dynamic Light Scattering Technique. *Toxicol. Sci.* **2008,** *101*, 239–253.
28. Scown, T. M.; Santos, E. M.; Johnston, B. D.; Gaiser, B.; Baalousha, M.; Mitov, S.; Lead, J. R.; Stone, V.; Fernandes, T. F.; Jepson, M.; *et al.* Effects of Aqueous Exposure to Silver Nanoparticles of Different Sizes in Rainbow Trout. *Toxicol. Sci.* **2010,** *115*, 521–534.
29. Lynch, I.; Salvati, A.; Dawson, K. A. Protein–Nanoparticle Interactions: What Does the Cell See? *Nat Nanotechnol.* **2009,** *4*, 546–547.
30. Liu, J.; Sonshine, D. A.; Shervani, S.; Hurt, R. H. Controlled Release of Biologically Active Silver from Nanosilver Surfaces. *ACS Nano* **2010,** *4*, 6903–6913.
31. Liu, J.; Hurt, R. H. Ion Release Kinetics and Particle Persistence in Aqueous Nano-Silver Colloids. *Environ. Sci. Technol.* **2010,** *44*, 2169–2175.

32. Luoma, S. N. Silver Nanotechnologies and the Environment: Old Problems or New Challenges? Woodrow Wilson International Centar for Scholars, 2008; p 66.
33. Hussain, S. M.; Hess, K. L.; Gearhart, J. M.; Geiss, K. T.; Schlager, J. J. *In Vitro* Toxicity of Nanoparticles in BRL 3A Rat Liver Cells. *Toxicol. In Vitro* **2005,** *19*, 975–983.
34. Braydich-Stolle, L.; Hussain, S.; Schlager, J. J.; Hofmann, M. C. *In Vitro* Cytotoxicity of Nanoparticles in Mammalian Germline Stem Cells. *Toxicol. Sci.* **2005,** *88*, 412–419.
35. Kawata, K.; Osawa, M.; Okabe, S. *In Vitro* Toxicity of Silver Nanoparticles at Noncytotoxic Doses to HepG2 Human Hepatoma Cells. *Environ. Sci. Technol.* **2009,** *43*, 6046–6051.
36. Kerneis, S.; Bogdanova, A.; Kraehenbuhl, J. P.; Pringault, E. Conversion by Peyer's Patch Lymphocytes of Human Enterocytes into M Cells That Transport Bacteria. *Science* **1997,** *277*, 949–952.
37. Leonard, F.; Collnot, E. M.; Lehr, C. M. A 3-Dimensional Co-Culture of Enterocytes, Macrophages and Dendritic Cells To Model the Inflamed Intestinal Mucosa *In Vitro*. *Mol. Pharmaceutics* **2010,** *7*, 2103–2119.
38. Hendriksen, P. J.; Dits, N. F.; Kokame, K.; Veldhoven, A.; van Weerden, W. M.; Bangma, C. H.; Trapman, J.; Jenster, G. Evolution of the Androgen Receptor Pathway during Progression of Prostate Cancer. *Cancer Res.* **2006,** *66*, 5012–5020.
39. Busch, W.; Kuhnel, D.; Schirmer, K.; Scholz, S. Tungsten Carbide Cobalt Nanoparticles Exert Hypoxia-Like Effects on the Gene Expression Level in Human Keratinocytes. *BMC Genomics* **2010,** *11*, 65.
40. Formigari, A.; Irato, P.; Santon, A. Zinc, Antioxidant Systems and Metallothionein in Metal Mediated-Apoptosis: Biochemical and Cytochemical Aspects. *Comp. Biochem. Physiol. C* **2007,** *146*, 443–459.
41. Park, E. J.; Yi, J.; Kim, Y.; Choi, K.; Park, K. Silver Nanoparticles Induce Cytotoxicity by a Trojan-Horse Type Mechanism. *Toxicol. In Vitro* **2010,** *24*, 872–878.
42. Kedziorek, D. A.; Muja, N.; Walczak, P.; Ruiz-Cabello, J.; Gilad, A. A.; Jie, C. C.; Bulte, J. W. Gene Expression Pprofiling Reveals Early Cellular Responses to Intracellular Magnetic Labeling with Superparamagnetic Iron Oxide Nanoparticles. *Magn. Reson. Med.* **2010,** *63*, 1031–1043.
43. Cortese-Krott, M. M.; Munchow, M.; Pirev, E.; Hessner, F.; Bozkurt, A.; Uciechowski, P.; Pallua, N.; Kroncke, K. D.; Suschek, C. V. Silver Ions Induce Oxidative Stress and Intracellular Zinc Release in Human Skin Fibroblasts. *Free Radical Biol. Med.* **2009,** *47*, 1570–1577.
44. Hultberg, B.; Andersson, A.; Isaksson, A. Metabolism of Homocysteine, Its Relation to the other Cellular Thiols and Its Mechanism of Cell Damage in a Cell Culture Line (Human Histiocytic Cell Line U-937). *Biochim. Biophys. Acta* **1995,** *1269*, 6–12.
45. Valko, M.; Rhodes, C. J.; Moncol, J.; Izakovic, M.; Mazur, M. Free Radicals, Metals and Antioxidants in Oxidative Stress-Induced Cancer. *Chem. Biol. Interact.* **2006,** *160*, 1–40.
46. Almofti, M. R.; Ichikawa, T.; Yamashita, K.; Terada, H.; Shinohara, Y. Silver Ion Induces a Cyclosporine a-Insensitive Permeability Transition in Rat Liver Mitochondria and Release of Apoptogenic Cytochrome *c*. *J. Biochem.* **2003,** *134*, 43–49.
47. Shaulian, E. AP-1—The Jun Proteins: Oncogenes or Tumor Suppressors in Disguise? *Cell Signal* **2010,** *22*, 894–899
48. Kitamura, M. Endoplasmic Reticulum Stress in the Kidney. *Clin. Exp. Nephro.l* **2008,** *12*, 317–325.
49. Qian, Y.; Tiffany-Castiglioni, E. Lead-Induced Endoplasmic Reticulum (ER) Stress Responses in the Nervous System. *Neurochem. Res.* **2003,** *28*, 153–162.
50. Olszewski, U.; Hamilton, G. Mechanisms of Cytotoxicity of Anticancer Titanocenes. *Anticancer Agents Med. Chem.* **2010,** *10*, 302–311.
51. Deli, M. A. Potential Use of Tight Junction Modulators to Reversibly Open Membranous Barriers and Improve Drug Delivery. *Biochim. Biophys. Acta* **2009,** *1788*, 892–910.
52. Tomita, M.; Hayashi, M.; Awazu, S. Absorption-Enhancing Mmechanism of EDTA, Caprate, and Decanoylcarnitine in Caco-2 Cells. *J. Pharm. Sci.* **1996,** *85*, 608–611.
53. Thijssen, V. L.; Hulsmans, S.; Griffioen, A. W. The Galectin Profile of the Endothelium: Altered Expression and Localization in Activated and Tumor Endothelial Cells. *Am. J. Pathol.* **2008,** *172*, 545–553.
54. Pellis, L.; Franssen-van Hal, N. L. W.; Burema, J.; Keijer, J. The Intraclass Correlation Coefficient Applied for Evaluation of Data Correction, Labeling Methods, and Rectal Biopsy Sampling in DNA Microarray Experiments. *Physiol. Genomics* **2003,** *16*, 99–106.
55. Tusher, V. G.; Tibshirani, R.; Chu, G. Significance Analysis of Microarrays Applied to the Ionizing Radiation Response. *Proc. Natl. Acad. Sci. U.S.A.* **2001,** *98*, 5116–5121.
56. Eisen, M. B.; Spellman, P. T.; Brown, P. O.; Botstein, D. Cluster Analysis and Display of Genome-Wide Expression Ppatterns. *Proc. Natl. Acad. Sci. U.S.A.* **1998,** *95*, 14863–14868.
57. Diehn, M.; Sherlock, G.; Binkley, G.; Jin, H.; Matese, J. C.; Hernandez-Boussard, T.; Rees, C. A.; Cherry, J. M.; Botstein, D.; Brown, P. O.; Alizadeh, A. A. SOURCE: A Unified Genomic Resource of Functional Annotations, Ontologies, and Gene Expression Data. *Nucleic Acids Res.* **2003,** *31*, 219–223.